

Solar differential rotation reproduced with high-resolution simulation

H. Hotta^{1*}, K. Kusano²

¹Department of Physics, Graduate School of Science, Chiba University,
1-33 Yayoi-cho, Inage-ku, Chiba 263-8522, Japan

²Institute for Space-Earth Environmental Research,
Nagoya University, Furo-cho, Chikusa-ku, Nagoya, Aichi 464-8601, Japan

*To whom correspondence should be addressed; E-mail: hotta@chiba-u.jp.

The Sun rotates differentially with a fast equator and slow pole[1]. Convection in the solar interior is thought to maintain the differential rotation. However, although many numerical simulations have been conducted to reproduce the solar differential rotation[2, 3, 4, 5, 6, 7], previous high-resolution calculations with solar parameters fall into the anti-solar (fast pole) differential rotation regime. Consequently, we still do not know the true reason why the Sun has a fast-rotating equator. While the construction of the fast equator requires a strong rotational influence on the convection, the previous calculations have not been able to achieve the situation without any manipulations. The problem is called convective conundrum[8]. The convection and the differential rotation in numerical simulations were different from the observations. Here, we show that a high-resolution calculation succeeds in reproducing the solar-like differential rotation. Our calculations indicate that the strong magnetic field generated by a small-scale dynamo has a significant impact on thermal convection. The successful reproduction of the differential rotation, convection, and magnetic field achieved in our calculation is an essential step to understanding the cause of the most basic nature of solar activity, specifically, the 11-year cycle of sunspot

activity.

In this study, we drastically increase the resolution using the Supercomputer Fugaku to investigate the possible influence of the magnetic field on the differential rotation. We perform three cases, Low, Middle, and High, where the numbers of grid points are $(N_r, N_\theta, N_\phi, N_{YY}) = (96, 384, 1156, 2)$, $(192, 768, 2312, 2)$, and $(384, 1536, 4608, 2)$, respectively. N_r , N_θ , and N_ϕ are the radial, latitudinal, and longitudinal grid points, respectively. N_{YY} is the factor from the Yin-Yang grid[9]. In the ordinary spherical grid, the numbers of grid points are $(N_r, N_\theta, N_\phi) = (96, 768, 1536)$, $(192, 1536, 3072)$, and $(384, 3072, 6144)$ in the Low, Middle, and High cases, respectively. Note that the resolution is fairly high even in the Low case compared with previous studies. We adopt solar stratification[10], solar rotation, and solar luminosity, and exclude any type of explicit diffusivity to maintain high resolution. Details of the numerical method are found in the Method section. We continue these calculations for 4000 days. The temporal evolutions of the energies are shown in Supplementary Figure 1.

Figure 1A and B shows three-dimensional volume rendering of the normalized entropy and the magnetic field strength in the High case, respectively. The maximum magnetic field strength exceeds 80 kG, which is a significant superequipartition magnetic field.

Figure 2 shows the dependence of the differential rotation on the resolution. Panels A, B, and C show the results for the Low, Middle, and High cases, respectively. In the Low case (Figure 2A), we obtain the fast pole and slow equator, which is consistent with previous studies. In the Middle case (Figure 2B), the differential rotation becomes more solar-like, while we still see a significant decrease of the angular velocity in the near-surface region around the equator. Even in the Middle case, the resolution is high as a long-term full spherical dynamo calculation. In the High case (Figure 2C), we nicely reproduce the solar-like differential rotation, specifically, the equator region is rotating faster than the pole. Similar to the real Sun, the topology of the differential rotation deviates from the Taylor–Proudman-like profile, i.e. the contour lines of our differential rotation are not aligned to the rotational axis. We do not force the entropy gradient at the bottom boundary[11], but the efficient small-scale dynamo increases

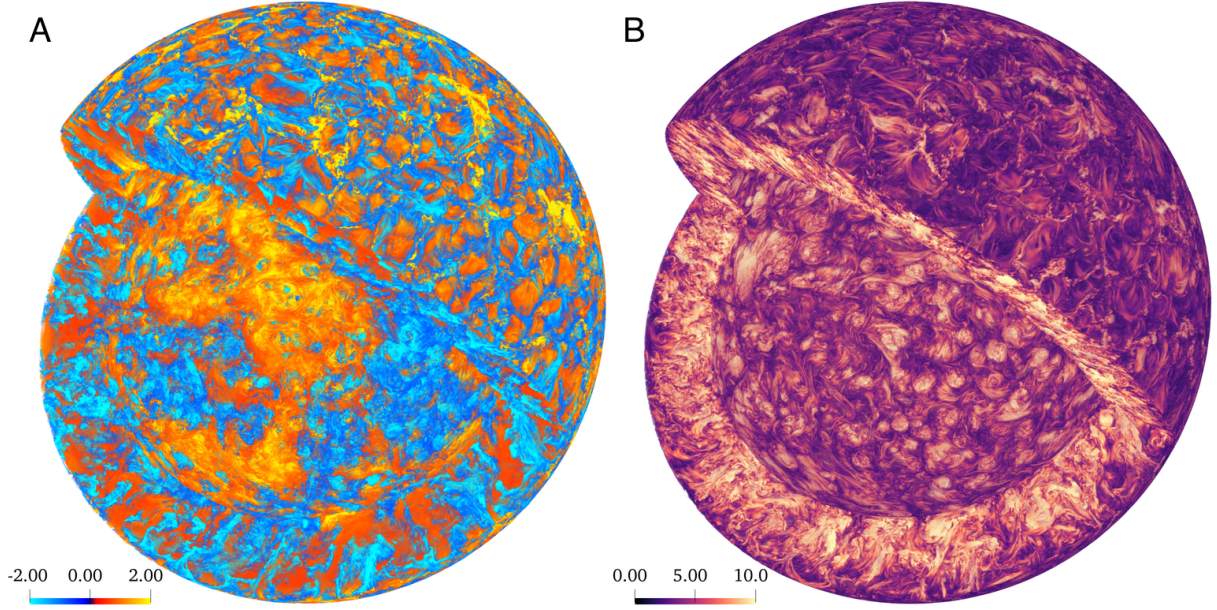


Figure 1: **Overall structure of convection and magnetic field.** Panels A and B show the normalized entropy and the magnetic field strength respectively. The magnetic field strength is shown in the unit of kG. A quadrant of sphere is striped to see the interior of the Sun.

the latitudinal entropy gradient as found by Hotta (2018)[7]. A differential rotation in a hydrodynamic calculation without the magnetic field is also shown in Supplementary Figure 3.

Figure 3 shows the convection and magnetic field properties. Panel A shows root-mean-square (RMS) velocity v_{RMS} . Higher resolution tends to show a smaller amplitude of the convection. The decrease in the convection velocity reduces the Rossby number. Figure 3B shows the RMS magnetic field (B_{RMS} : solid line) and equipartition magnetic field (B_{eq} : dotted line), where $B_{\text{eq}} = \sqrt{4\pi\rho_0 v_{\text{RMS}}}$ and ρ_0 is the background density. The RMS magnetic fields monotonically increase with the resolution. In the Low case, the magnetic field is always smaller than the equipartition magnetic field. In previous studies, the RMS magnetic field reaches 10–20% of the equipartition magnetic field[12]. The system reaches an efficient small-scale dynamo regime even in the Low case because the magnetic field achieves an almost equipartition level. In the Middle case, the superequipartition magnetic field ($B_{\text{RMS}} > B_{\text{eq}}$) is reproduced in the bottom half of the convection zone. In the High case, the magnetic energy exceeds the kinetic

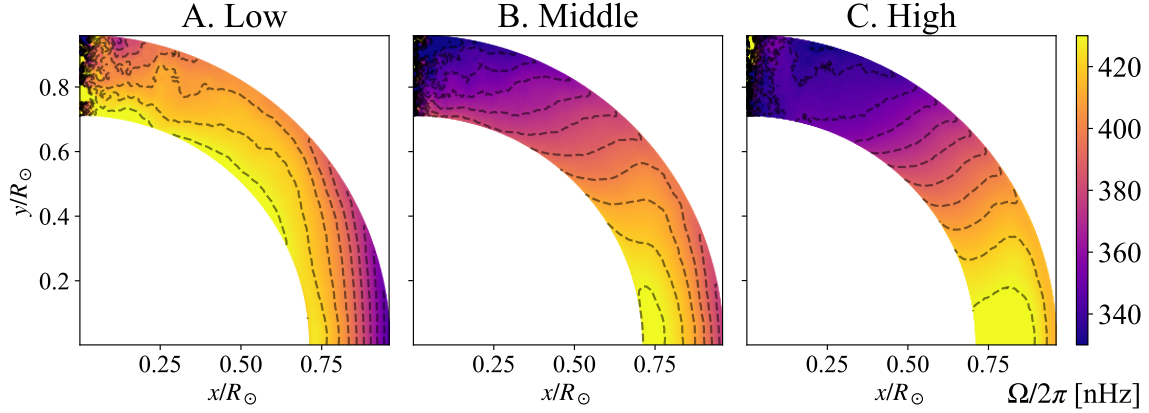


Figure 2: **Dependence of differential rotation on the resolution.** Panels A, B, and C show the results from the Low, Middle, and High cases, respectively. The value $\Omega/2\pi$ is shown in units of nHz, where Ω is the angular velocity. The dashed lines show the values from 330 to 430 nHz in 10 nHz increments. The results in the northern and southern hemispheres are averaged.

energy in all layers in the convection zone. This strong magnetic field suppresses the convection velocity significantly. In the High case, the stretching becomes weaken and the compression increases. The generation mechanism of the magnetic field is discussed also in Supplementary Figures 4 and 5.

Figure 4 shows the kinetic (solid line) and magnetic (dotted line) energy spectra at $r = 0.83R_{\odot}$. In the Low case, the magnetic energy exceeds the kinetic energy only on a small scale ($\ell > 100$). This is a clear sign of the efficient small-scale dynamo[13]. In the Middle case, the turnover scale of the superequipartition magnetic field moves to a larger scale ($\ell \sim 45$). While in the small scale ($\ell > 10$), the kinetic energy in the Middle case is smaller than that of the Low case because of stronger Lorentz force feedback, the kinetic energy does not change in the large-scale ($\ell < 10$). In the High case, the magnetic energy exceeds the kinetic energy on almost all the scales. The kinetic energy is also reduced in all the scales. Because of this kinetic energy suppression in the High case, the peak of the kinetic energy is shifted from $\ell \sim 6$ (Low and Middle cases) to $\ell \sim 30$. These spectra variations indicate that the dynamo in the High case is qualitatively different from the others.

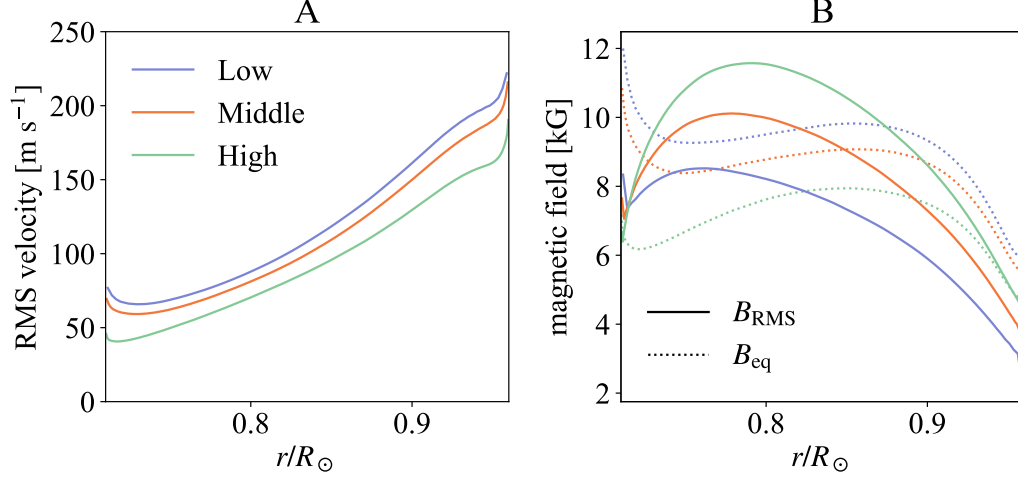


Figure 3: **Dependence of the convection and magnetic field properties on the resolution.** Panel A shows the RMS velocity, and panel B shows the RMS (solid lines) and equipartition (dotted lines) magnetic field strengths. The blue, orange, and green lines show the results from the Low, Middle, and High cases, respectively.

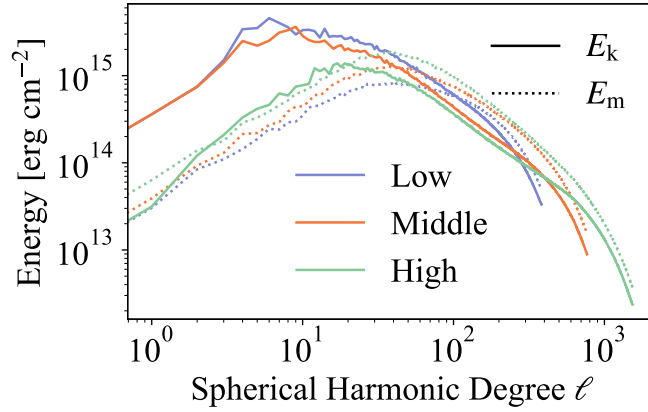


Figure 4: **Dependence of kinetic and magnetic energy spectra on the resolution.** The spectra at $r = 0.83R_\odot$ are shown. The solid and dotted lines show the kinetic and magnetic energy spectra, respectively. The blue, orange, and green lines show the spectra in Low, Middle, and High cases, respectively. In this plot, only the $m \neq 0$ mode is shown to exclude contributions from the differential rotation, where m is the spherical harmonic order.

Discussion

In this study, we reproduce the solar-like differential rotation in an high-resolution calculation with solar parameters, such as the stratification, the luminosity, and the rotation rate. Our calculation results show that the Sun has a marginal Rossby number between anti-solar (fast pole) and solar-like (fast equator) differential rotation, and we need a sophisticated treatment of the thermal convection and the magnetic field to reproduce the differential rotation. We offer a path forward in resolving the convective conundrums. Significant reduction in the convective energy in the large-scale ($\ell < 30$) is a promising trend to solve the other part of the convective conundrum, i.e. the energy spectra obtained by helioseismology[14]. Because the observational result for the energy spectra is still controversial, detailed comparisons between numerical simulations and observations are needed to solve the problem. Furthermore, by appropriately reproducing the differential rotation, the convection will lead to a correct understanding of the generation of the large-scale magnetic field and cycle. In this study, the dynamo has not constructed the large-scale magnetic field (see Supplementary Figure 2) probably due to lack of the calculation time for the large-scale dynamo or the insufficient suppression of the convection velocity. It is possible that the longer time calculation changes the amplitude of the magnetic field. This is still out of our reach. In addition, we have not reached the numerical convergence where the result does not change with doubling the resolution. We cannot rule out the further change of the differential rotation in higher-resolution simulations. We expect the further resolution leads to a stronger magnetic field which more suppresses the convection velocity. This is a good factor for the construction of the large-scale magnetic field as well. The higher resolution simulation is still on demand.

References

- [1] Schou, J. *et al.* Helioseismic Studies of Differential Rotation in the Solar Envelope by the Solar Oscillations Investigation Using the Michelson Doppler Imager. *Astrophys. J.* **505**, 390–417 (1998).

- [2] Miesch, M. S. *et al.* Three-dimensional Spherical Simulations of Solar Convection. I. Differential Rotation and Pattern Evolution Achieved with Laminar and Turbulent States. *Astrophys. J.* **532**, 593–615 (2000).
- [3] Brown, B. P., Browning, M. K., Brun, A. S., Miesch, M. S. & Toomre, J. Rapidly Rotating Suns and Active Nests of Convection. *Astrophys. J.* **689**, 1354–1372 (2008).
- [4] Nelson, N. J., Brown, B. P., Brun, A. S., Miesch, M. S. & Toomre, J. Magnetic Wreaths and Cycles in Convective Dynamos. *Astrophys. J.* **762**, 73 (2013).
- [5] Hotta, H., Rempel, M. & Yokoyama, T. High-resolution Calculation of the Solar Global Convection with the Reduced Speed of Sound Technique. II. Near Surface Shear Layer with the Rotation. *Astrophys. J.* **798**, 51 (2015).
- [6] Hotta, H., Rempel, M. & Yokoyama, T. Large-scale magnetic fields at high Reynolds numbers in magnetohydrodynamic simulations. *Science* **351**, 1427–1430 (2016).
- [7] Hotta, H. Breaking Taylor-Proudman Balance by Magnetic Fields in Stellar Convection Zones. *Astrophys. J.* **860**, L24 (2018).
- [8] O’Mara, B., Miesch, M. S., Featherstone, N. A. & Augustson, K. C. Velocity amplitudes in global convection simulations: The role of the Prandtl number and near-surface driving. *Advances in Space Research* **58**, 1475–1489 (2016).
- [9] Kageyama, A. & Sato, T. “Yin-Yang grid”: An overset grid in spherical geometry. *Geochemistry, Geophysics, Geosystems* **5**, Q09005 (2004).
- [10] Christensen-Dalsgaard, J. *et al.* The Current State of Solar Modeling. *Science* **272**, 1286–1292 (1996).
- [11] Miesch, M. S., Brun, A. S. & Toomre, J. Solar Differential Rotation Influenced by Latitudinal Entropy Variations in the Tachocline. *Astrophys. J.* **641**, 618–625 (2006).

- [12] Fan, Y. & Fang, F. A Simulation of Convective Dynamo in the Solar Convective Envelope: Maintenance of the Solar-like Differential Rotation and Emerging Flux. *Astrophys. J.* **789**, 35 (2014).
- [13] Hotta, H., Rempel, M. & Yokoyama, T. Efficient Small-scale Dynamo in the Solar Convection Zone. *Astrophys. J.* **803**, 42 (2015).
- [14] Hanasoge, S. M., Duvall, T. L. & Sreenivasan, K. R. Anomalously weak solar convection. *Proceedings of the National Academy of Science* **109**, 11928–11932 (2012).
- [15] Hotta, H., Rempel, M. & Yokoyama, T. High-resolution Calculations of the Solar Global Convection with the Reduced Speed of Sound Technique. I. The Structure of the Convection and the Magnetic Field without the Rotation. *Astrophys. J.* **786**, 24 (2014).
- [16] Hotta, H., Iijima, H. & Kusano, K. Weak influence of near-surface layer on solar deep convection zone revealed by comprehensive simulation from base to surface. *Science Advances* **5**, eaau2307 (2019).
- [17] Hotta, H. & Iijima, H. On rising magnetic flux tube and formation of sunspots in a deep domain. *Mon. Not. R. Astron. Soc.* **494**, 2523–2537 (2020).
- [18] Hotta, H., Rempel, M., Yokoyama, T., Iida, Y. & Fan, Y. Numerical calculation of convection with reduced speed of sound technique. *Astron. Astrophys* **539**, A30 (2012).
- [19] Rempel, M. Numerical Simulations of Quiet Sun Magnetism: On the Contribution from a Small-scale Dynamo. *Astrophys. J.* **789**, 132 (2014).

Acknowledgments

We appreciate T. Yokoyama, R. Shimada and T. Hanawa for insightful comments on the manuscript. The results were obtained using the Supercomputer Fugaku provided by the RIKEN Center for Computational Science, the Supercomputer Flow at Nagoya University, and the Cray XC50 provided by the Center for

Computational Astrophysics, National Astronomical Observatory of Japan. Funding: This work was supported by MEXT/JSPS KAKENHI (grant no. JP20K14510 (PI: H. Hotta), JP21H04492 (PI: K. Kusano), JP21H01124 (PI: T. Yokoyama), JP21H04497 (PI: H. Miayahara)) and MEXT as a Program for Promoting Researches on the Supercomputer Fugaku (Toward a unified view of the universe: from large-scale structures to planets, grant no. 20351188 (PI: J. Makino)).

Authors contributions

H.H. contributed to the design of the project, developed the numerical code, carried out simulations, performed analysis, and wrote the first draft of the paper. K.K. contributed to the design of the project, interpretation of the result, and writing of the final draft.

Competing interests

The authors declare no competing interest.

Methods

Data availability

We have opted not to make R2D2 code publicly available. Running R2D2 code requires expert assistance and appropriate computer system. The numerical method is explained in our previous publication in detail[15, 5]. The data generated, analysed, and presented in this study are available at <https://doi.org/10.5281/zenodo.5003258>.

Numerical simulation

We solve the three-dimensional magnetohydrodynamic equations in spherical geometry (r, θ, ϕ) with an extended version of the R2D2 code[16, 17]. The equations for the calculation are:

$$\frac{\partial \rho_1}{\partial t} = -\frac{1}{\xi^2} \nabla \cdot (\rho \mathbf{v}), \quad (1)$$

$$\frac{\partial}{\partial t} (\rho \mathbf{v}) = -\nabla \cdot (\rho \mathbf{v} \mathbf{v}) - \nabla p_1 - \rho_1 g \mathbf{e}_r + \frac{1}{4\pi} (\nabla \times \mathbf{B}) \times \mathbf{B} + 2\rho \mathbf{v} \times \boldsymbol{\Omega}_0 \quad (2)$$

$$\frac{\partial \mathbf{B}}{\partial t} = \nabla \times (\mathbf{v} \times \mathbf{B}), \quad (3)$$

$$\rho T \frac{\partial s_1}{\partial t} = -\rho T (\mathbf{v} \cdot \nabla) s + Q_{\text{rad}}, \quad (4)$$

$$p_1 = \left(\frac{\partial p}{\partial \rho} \right)_s \rho_1 + \left(\frac{\partial p}{\partial s} \right)_\rho s_1, \quad (5)$$

where ρ , \mathbf{v} , \mathbf{B} , s , T , g , $\boldsymbol{\Omega}_0$, and Q_{rad} are the density, the fluid velocity, the magnetic field, the specific entropy, the temperature, the gravitational acceleration, the system rotation, and the radiative heating. ξ is the factor from the reduced speed of sound technique[18]. The subscript 1 indicates the perturbation from the zeroth order spherically symmetric background from the Model S[10]. For the detailed method, the readers can find information in our previous publications[15, 5]. In this study, the calculation domain extends from $0.71R_\odot$ to $0.96R_\odot$ in the radial direction. The whole sphere is covered with the Yin-Yang grid [9]. The equations are solved with the fourth-order space-centred method and four-step Runge–Kutta method for time integration. We do not include any explicit diffusivity, and only the artificial viscosity with slope limiter[19] is used. Non-penetrative and stress-free boundary conditions are used for the top and bottom boundaries. The horizontal and vertical magnetic field boundary conditions are used at the bottom and top boundaries, respectively.

We average quantities in the period from 3600 to 4000 days to show the results.

Normalization of energy spectra

We adopt a standard way to normalize the energy spectra adopted in our field. When the RMS velocity $v_{\text{RMS}}(r)$ and magnetic field $B_{\text{RMS}}(r)$ are defined, the kinetic E_k and magnetic E_m energy spectra are

normalized to satisfy the relation:

$$\frac{1}{2}\rho_0 v_{\text{RMS}}^2 = \sum_{\ell>0} \frac{E_{\text{k}}(\ell)}{r}, \quad (6)$$

$$\frac{B_{\text{RMS}}^2}{8\pi} = \sum_{\ell>0} \frac{E_{\text{m}}(\ell)}{r}. \quad (7)$$